Asian Journal of Chemistry; Vol. 37, No. 5 (2025), 1111-1117

ASIAN JOURNAL OF CHEMISTRY

https://doi.org/10.14233/ajchem.2025.33562

Enhancing Solar Cell Efficiency with GaAs/$Al_{0.3}Ga_{0.7}As$ Systems: Electronic and Optical Properties Analysis

A. HMAIRROU[1], E.H. CHAHID[1,2,3], M. AZZA[1], Y. RACHDI[1,*], N. JARMOUNI[1], A. AMINE[3,4], Y. MIR[3], M. ZAZOUI[3], A. MALAOUI[2] and S. BELAAOUAD[1]

[1]Laboratory of Physical Chemistry of Applied Materials, Faculty of Sciences Ben M'Sik, Hassan II University of Casablanca, B.P. 7955, Bd Cdt Driss El Harti, Casablanca, Morocco
[2]Research Laboratory in Physics and Sciences for Engineers, Polydisciplinary Faculty, Sultan Moulay Slimane University, Beni Mellal, Morocco
[3]Laboratory of Materials, Energy and Control Systems, FST Mohammedia, Hassan II University of Casablanca, B.P. 7955, Bd Cdt Driss El Harti, Casablanca, Morocco
[4]Laboratory of Instrumentation Measurements and Control, Chouaib Doukkali University, El Jadida, Morocco

*Corresponding author: E-mail: rachdi.smc@gmail.com

Received: 24 February 2025; *Accepted*: 31 March 2025; *Published online*: 30 April 2025; AJC-21977

This study aims to enhance the optical and electrical performance of GaAs (gallium arsenide) solar cells by incorporating p-type and n-type $Al_{0.3}Ga_{0.7}As$ layers. The physical parameters were simulated by using density functional theory (DFT) through generalized gradient approximation (GGA) for potential exchange-correlation from implementation Win2K code. The SCAPS software and impedance spectroscopy method were also used to investigate the solar cell characteristics. Our findings demonstrate that adding these layers significantly improves efficiency by 31% compared to a standard GaAs pin-junction structure. This enhancement is attributed to optimized light absorption and reflection through doping, leading to a high-performance solar cell.

Keywords: Gallium-Arsenide solar cells, Electronic properties, Optical properties, Doping, Impedance spectroscopy.

INTRODUCTION

As fossil fuels and related equipment became more expensive, people became interested in renewable energy sources [1], particularly solar energy [2]. The primary advantages of solar energy that sparked significant interest at the time were its cost-free nature, widespread availability across the globe and its clean and inexhaustible supply compared to fossil fuels. The improvement of solar energy utilization will be linked not primarily to its financial benefits (which can increase as fossil fuel savings decrease) [3], but rather to overall national security considerations: no polluting emissions (smoke containing CO_2 and NOx from thermal power plants), no radioactive hazards and no bulky waste (nuclear power plants) and the possibility of limiting chlorofluorocarbons (CFCs) usage (cold generation by absorption).

Solar energy is mainly utilized in several ways, including photovoltaic conversion, which directly converts radiation into electrical current using solar cells. In fact, various types of structures have been developed for solar cell applications employing distinct advanced materials, such as GaAs (gallium arsenide) solar cells and its derivatives [3]. The gallium arsenide GaAs compounds have been broadly utilized in later decades, especially in space applications, since of their execution compared to silicon-based solar cells, in specific their high efficiency, as well as the points of interest of adaptability and softness. Nevertheless, one challenge was the rate of surface recombination, which primarily limited the efficiency of early GaAs-based cells to around 10% [4]. The addition of $Al_{1-x}Ga_xAs$ (aluminum gallium arsenide) window layers to the GaAs surface was one partial solution to this problem. Today, these solar cells have achieved efficiencies exceeding 25%.

The ternary material $Al_{0.3}Ga_{0.7}As$ is widely applied to the construction of multi-junction structures [5]. The interface properties between GaAs and $Al_{0.3}Ga_{0.7}As$ play an important role in the electronic and optical qualities of the formed structures

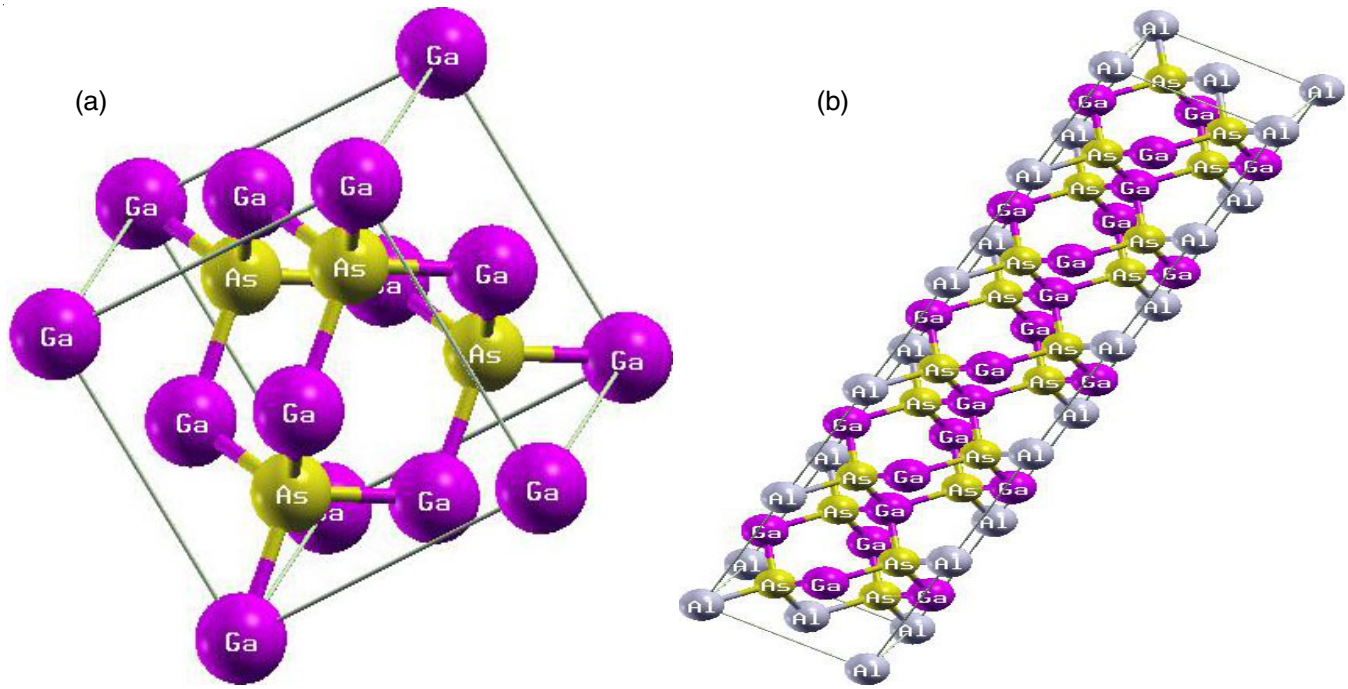

Fig. 1. 3D geometry optimized structure of GaAs doped with aluminium (30%): (a) supercell 1 × 1 × 1, (b) supercell 1 × 1 × 5

[6]. The GaAs/$Al_{0.3}Ga_{0.7}As$ systems have garnered significant attention from researchers due to their lattice constant difference exceeding 0.14% [7]. The metal-organic chemical vapour deposition (MOCVD) and molecular beam epitaxy (MBE) are the preferred methods for producing high-quality $Al_{0.3}Ga_{0.7}As$ surfaces. Recent studies have linked the superior performance of $Al_{0.3}Ga_{0.7}As$/GaAs heterostructures to their exceptional optical and electronic properties [8]. This work focuses on a comprehensive analysis of the optical and electronic properties of GaAs and $Al_{0.3}Ga_{0.7}As$, as well as the GaAs/$Al_{0.3}Ga_{0.7}As$ systems, specifically for applications in solar cells.

COMPUTATIONAL METHODS

Structural, electronic and optical properties: The physical characteristics of $Al_{0.3}Ga_{0.7}As$ and GaAs were investigated *via* density functional theory (DFT) [9] using the GW approach [10], starting from implementation (WIEN2k code) [11]. We also used Tran-Blaha modified Becke-Johnson (TB-mBJ) exchange potential approximation, the calculation gives 120 K-points which is equivalent to 1000 K-points in the first Brillouin zone (BZ) with a mesh (10 × 10 × 10) k points corresponding. To get energy convergence, the parameter $R_{MT}K_{max}$ was set to 7, where R_{MT} denotes the smallest atomic sphere radius and K_{max} is the magnitude of the largest k plane wave vector. The energy convergence scale was set to (0.0001 Ry) for each calculation. The other charge density and potential parameters were extended from Fourier up to $G_{max} = 12(Ryd)^{1/2}$. The operation of the initial supercell P 1 × 1 × 1 in DFT simulations makes all the sites inequivalent in the GaAs structure (space group *Fm3m*; $a = b = c = 5.75$ Å; $\alpha = \beta = \gamma = 90^{o}$) as presented in Fig. 1. As a result, the $Al_{0.3}Ga_{0.7}As$ exhibits 8 atoms, which are 2 Ga and 2As atoms. Subsequently, we replace gallium atoms with aluminum up to 30% doping in the supercell (1 × 1 × 5).

To study the electronic proprieties, we have used the approximation for exchange and correlation terms (mBJ-GG) approximation along the directions of high symmetry in the Brillouin zone (BZ), calculated at the Γ(0,0,0,0) point for the GaAs and $Al_{0.3}Ga_{0.7}As$. The optical properties were examined in terms of absorption and refraction. The absorption coefficient α of the materials studied depends on the electronic transitions of an electron located in an energy level and the reflectivity index R elucidates the dispersion of light and transparent behaviour of the material.

GaAs solar cell examination: This work aims principally to simulate solar cells based on GaAs/$Al_{0.3}Ga_{0.7}As$ systems using the SCAPS software and estimate the optimum parameters to design such a solar cell with high efficiency. The structure of the considered solar cell is represented in Fig. 2 and mainly consists of a GaAs-based cell, in which the p-$Al_{0.3}Ga_{0.7}As$ window layer (FSF) has been deposited on p-GaAs layer and the n-$Al_{0.3}Ga_{0.7}As$ layer (BSF) is inserted between the n-GaAs layer and the substrate [12].

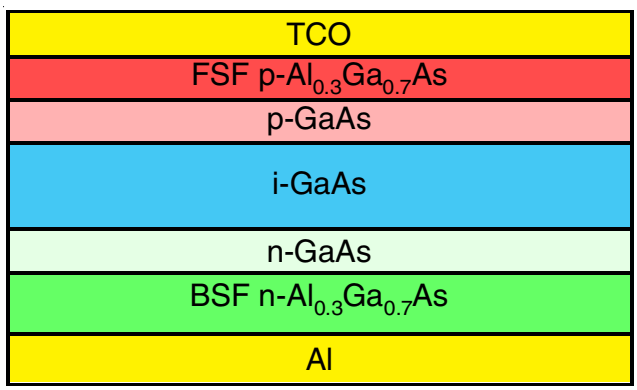

Fig. 2. Schematic structure of p-i-n solar cell

To optimize this solar cell design using SCAPS software, several key physical parameters were employed as outlined in Table-1. The SCAPS-1D software applied in this work is capable of simulating both AC and DC electrical behaviour in solar cells and displaying the results. For DC simulations, it provides key performance indicators such as short-circuit current, open-circuit voltage, fill factor and conversion efficiency through current-voltage curves. In AC simulations, the software generates complex impedance data at various frequencies. Both types of simulations (AC and DC) are used to investigate the considered solar cell. The electrical, optical and impedance properties are generated and analyzed in order to optimize the solar cell efficiency.

RESULTS AND DISCUSSION

Electronic properties of GaAs and $Al_{0.3}Ga_{0.7}As$: As shown in Fig. 3, the band structures of GaAs and $Al_{0.3}Ga_{0.7}As$ are between -14.0 and 8.0 eV calculated with TB-mBJ approximation. The direct band gaps are 1.24 eV and 1.61eV of GaAs and $Al_{0.3}Ga_{0.7}As$, respectively. The substitution of the gallium atom with aluminum leads to an increase in the band gap as a result of the difference in existing energy between the valence band and conduction band, due to the charge transfer between Al, Ga and As. It should be observed that the system keeps the symmetrical structure, with a direct band gap.

Optical properties of GaAs and $Al_{0.3}Ga_{0.7}As$: The extent to which light is absorbed by the substance is influenced by the movement of its electrons across different energy states. Moreover, the ability of the material to bend light and its transparency are revealed by its refractive index. The absorption spectrum of the GaAs and $Al_{0.3}Ga_{0.7}As$ are shown in Fig. 4a. Their optical behaviour is extensive and becomes significant in the range of 4.5 to 8 eV, which means that both GaAs and $Al_{0.3}Ga_{0.7}As$ have higher absorption in the ultraviolet region [13]. These properties are recommended to use these materials in the photovoltaic. The reflectivity R spectrum is shown in

TABLE-1
PARAMETERS UTILIZED TO SIMULATE THE GaAs p-i-n SOLAR CELL WITH FRONT SURFACE FIELD (FSF) AND BASE SURFACE FIELD (BSF)

Parameters	FSF ($Al_{0.3}Ga_{0.7}As$)	p-GaAs	i-GaAs	Negas	BSF ($Al_{0.3}Ga_{0.7}As$)
Thickness (nm)	20	150-200	490	200-20	40
Dielectric perm (ε_r)	12.048	12.4	12.4	12.4	12.048
Affinity, χ_e (eV)	3.740	4.07	4.07	4.07	3.740
Band gap, E_g (eV)	1.803	1.24	1.24	1.24	1.803
Electron mobility, μ_e ($cm^2\ V^{-1}\ s^{-1}$)	2300	8500	8500	8500	2300
Hole mobility, μ_h ($cm^2\ V^{-1}\ s^{-1}$)	145.6	400	400	400	145.6
DOSCB: N_C (cm^{-3})	6.5×10^{17}	1×10^{18}	1×10^{18}	1×10^{18}	6.5×10^{17}
DOSVB: N_V (cm^{-3})	1.12×10^{19}	1.00×10^{19}	1.00×10^{19}	1.00×10^{19}	1.12×10^{19}
Acceptor concentration, N_A (cm^{-3})	2.00×10^{18}	2.00×10^{18}–1.00×10^{19}	0	0	0
Donor concentration, N_D (cm^{-3})	0	0	0	2.00×10^{18}	2.00×10^{18}

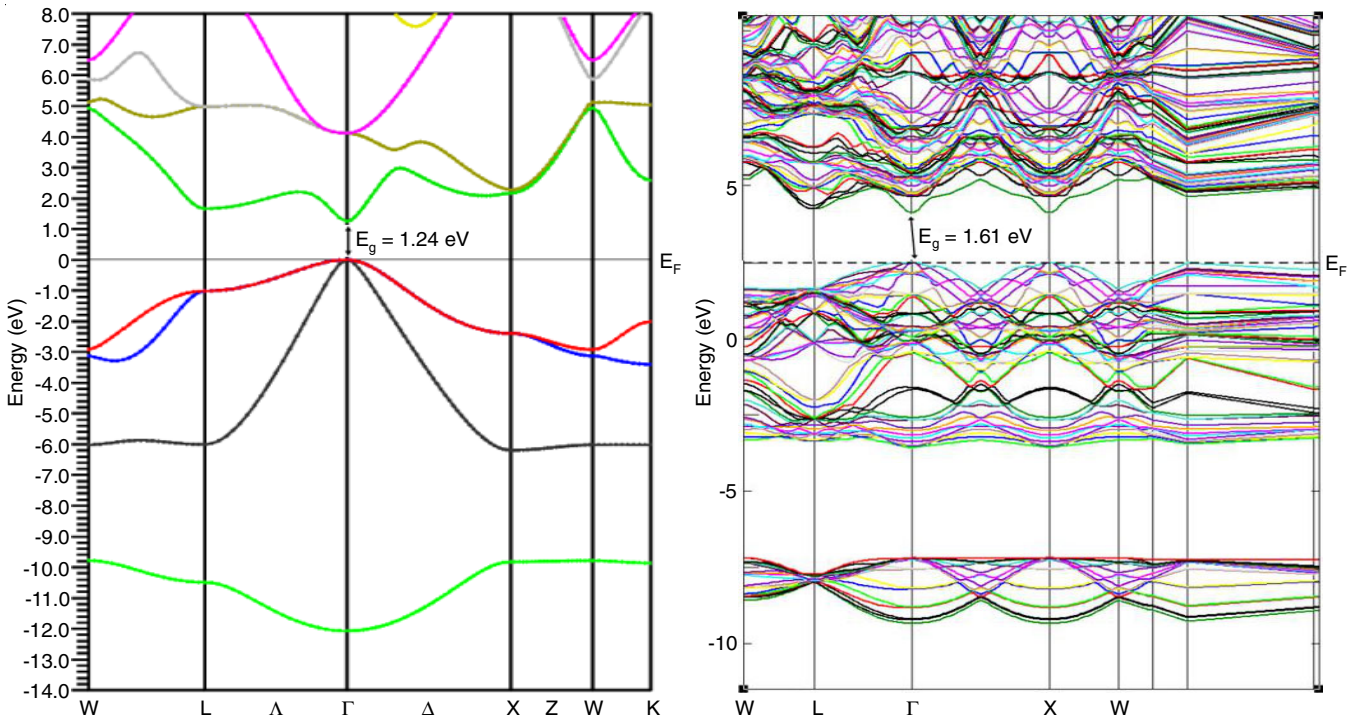

Fig. 3. The band structures of GaAs and $Al_{0.3}Ga_{0.7}As$ calculated by (TB-mBJ) potential

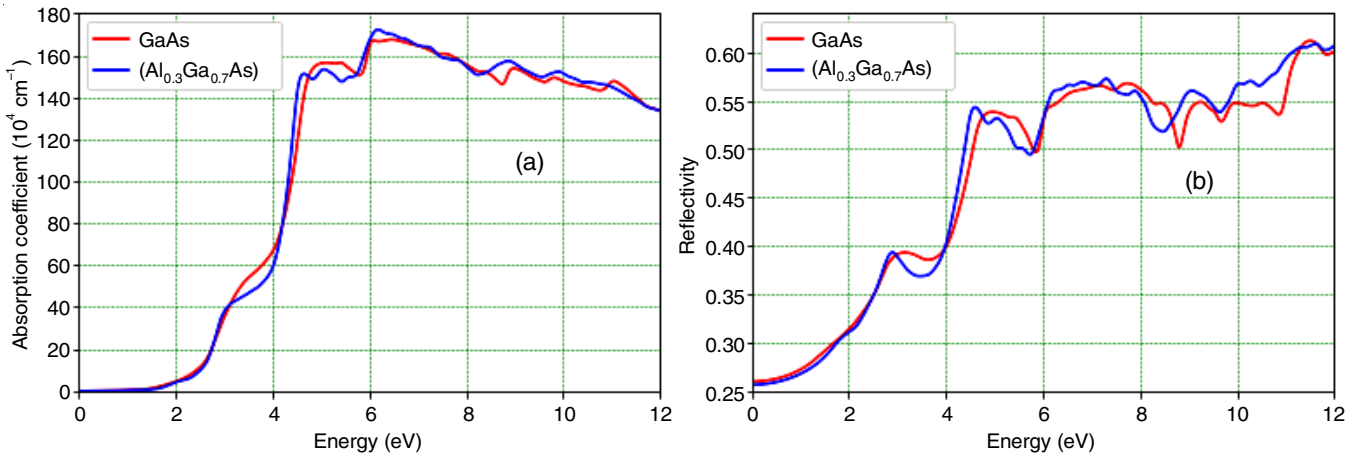

Fig. 4. (a) The absorption coefficient and (b) the reflectivity spectrums calculated by (mBJ) potential for GaAs (red line) and $Al_{0.3}Ga_{0.7}As$ (blue line)

Fig. 4b. The R(0) is 26% and 25 % for GaAs and $Al_{0.3}Ga_{0.7}As$, respectively. The maximum reflectivity value is 39.3% at 3.2 eV and 2.9 eV for GaAs and $Al_{0.3}Ga_{0.7}As$, respectively in visible light. The small matter of reflectivity and the absorptivity in the infrared region indicates that both compounds are transparent in this range.

Electrical parameters of solar cell: There are a few fundamental electrical parameters that characterize a photovoltaic cell, counting short-circuiting current (ISC), open-circuit voltage (V_{OC}), form factor (FF), efficiency (η) and spectral response. Among them η and FF parameters are the specific intrigued in this study [14,15]. The efficiency η characterizes the capacity of a photovoltaic cell to convert incident radiation into electrical current and is given by the ratio between the maximum power and the light power generated by the photovoltaic cell [13]:

$$\eta = \frac{P_m}{ES} \quad (1)$$

where E is the illuminance (W/m^2) and S is the cell surface (m^2).

Under standard test conditions (STC) 1 for solar panels, which are characterized by solar radiation of 1000 W/m^2, a solar spectrum AM 1, 5 and 25 ºC ambient temperature, the maximum power is called peak power (P_c). Efficiency is expressed as follows [16]:

$$\eta = \frac{P_c}{1000.S} \quad (2)$$

There are many technologies available on the market [17], with crystalline and amorphous silicon accounting for over 80% of global market for terrestrial applications, with efficiencies from 15 to 20% STC for crystalline silicon and from 5 to 12% for amorphous silicon [18]. Gallium arsenide (GaAs)-based photovoltaic cells, generally designed for space applications, has efficiencies ranging from 25 to 40% [19]. Photovoltaic cells are also characterized, as mentioned above, by another parameter called the form factor (FF) defined by the ratio between the maximum power and the power formed by the rectangle $J_{SC} \times V_{CO}$ [20]:

$$\text{Form factor (FF)} = \frac{P_m}{J_{SC} \times V_{OC}} \quad (3)$$

This factor is a signal of the quality of photogenerator, as well as the nature of resistances operating in the cell if they are in series or parallel. The optimal solar cell performance is achieved as the form factor nears 100% [21]. In the following parts, all these parameters were investigated in our case as a function of $Al_xGa_{1-x}As$ layer, doping and temperature effects.

Effect of $Al_xGa_{1-x}As$ layer using SCAPS-1D: The parameters utilized for the GaAs-based p-i-n solar cell at T = 300 K are recorded in Table-1. The results of the GaAs solar cell junction types using SCAPS-1D are summarized in Table-2 and Fig. 5. All through the reenactment, the standard solar cell conditions are AM 1.5 at 300 K and 1000 W/m^2 irradiance. The existence of the two windows (BSF) and (FSF) allows amplifying the photovoltaic cell's performance. Consequently, the form factor can exceed 90% and the efficiency can reach 31%.

TABLE-2
SIMULATED CELL PARAMETERS AS A FUNCTION OF STRUCTURE TYPE

Structure type	V_{co} (V)	J_{cc} (mA/cm^2)	FF (%)	η (%)
Without FSF and BSF	1.02	28.95	88.35	26.10
With FSF and BSF	1.29	26.29	90.35	30.67

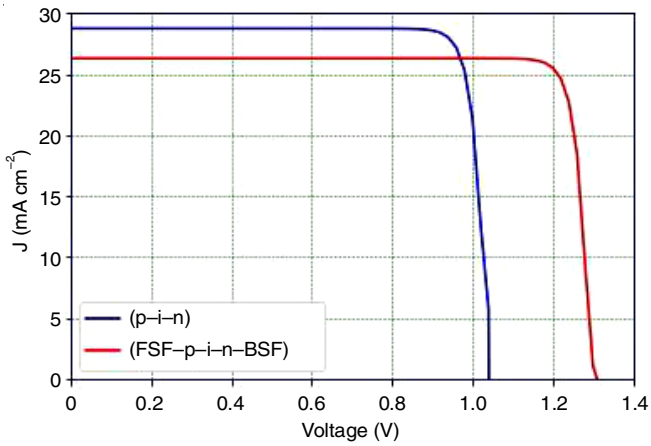

Fig. 5. Effect of the FSF and BSF on the (J–V) characteristic

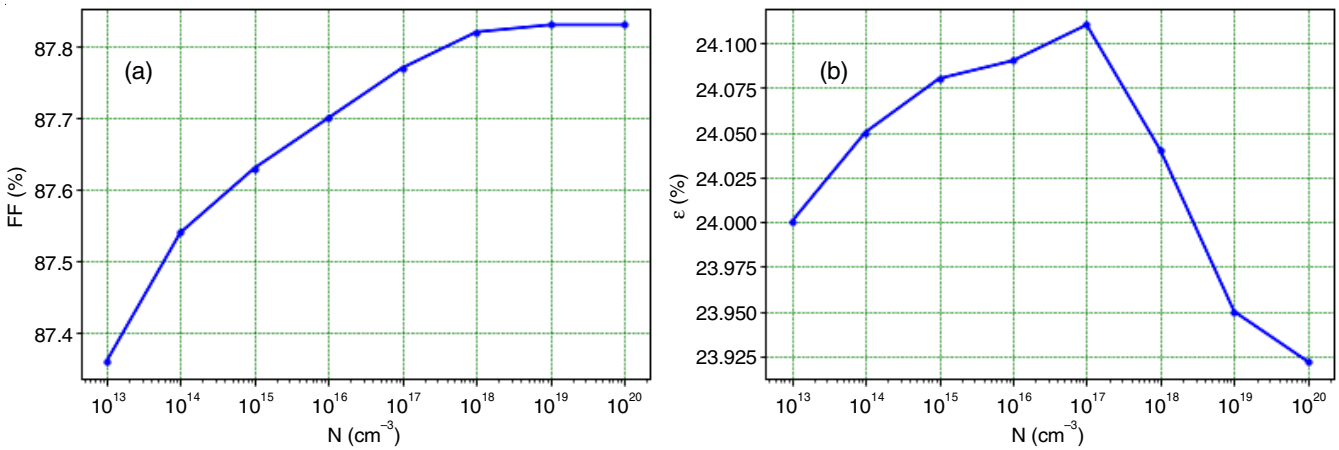

Fig. 6. Effect of doping on solar cell performance

Doping effect: The effect of window layer doped on form factor and efficiency are shown in Fig. 6. The form factor increases with increasing doping content. As well, the yield with doping until reaches the maximum at N = 10^{17} cm^{-3}, then decreases once this value is exceeded.

Temperature effect: Solar cells are used almost everywhere in the world and now also on other planets, such as Mars and the climatic conditions vary throughout the year. Thereby leads to fluctuations in the operating temperature of the photovoltaic cell. Therefore, their performance will be strongly influenced. We studied the effect of temperature, whereas the other parameters remained unchanged. The achieved results are illustrated in Table-3, Figs. 7 and 8.

TABLE-3
SIMULATED CELL PARAMETERS AS A FUNCTION OF TEMPERATURE TYPE

Temp. (K)	V_{co} (V)	J_{cc} (mA/cm^2)	FF (%)	η (%)
273.15	1.3590	25.92	91.33	32.19
283.15	1.3403	25.92	90.99	31.61
303.15	1.3014	25.92	90.29	30.46
323.15	1.2623	25.92	89.56	29.31
343.15	1.2228	25.92	88.80	28.15

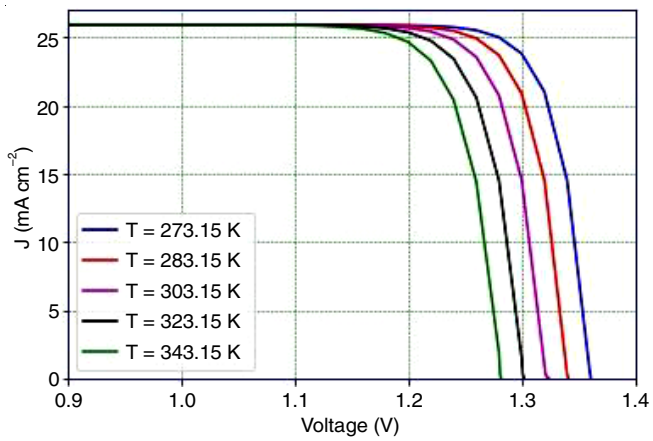

Fig. 7. Effect of temperature on the (J–V) characteristic

The increase in the temperature leads to a relative reduction in the performance of the photovoltaic cell, whose efficiency decreases from 32.19% at T = 273 K to 28.15% at T = 343 K. This reduction can be explained by decreasing the other main electrical parameters, the open-circuit voltage; and form factor. The V_{OC} decreased from 1.359 V to 1.2228 V by increasing the temperature from 273 K to 343 K, respectively.

Impedance spectroscopy method: Impedance spectroscopy method (ISM) is a powerful method extensively used for characterization of a wide range of electronic materials and photovoltaic devices [11,22]. This versatile method allows for evaluating cell performance by measuring electrical characteristics such as resistance and capacitance [23]. Furthermore, it offers a deeper understanding of the movement and distribution of charges within the semiconductor substance. Certainly, the impedance parameters acquired from the AC simulation utilizing SCAPS-1D software are illustrated in Fig. 9a-b. As can be seen, in the low frequency regime, the impedance complex is characterized by a semicircle for each frequency and can be modeled as a resistor R_s, a parallel connection of a resistor R_p and a capacitor C. The theoretical analysis of front surface field (FSF) and base surface field (BSF) provides the electrical values which are 0.285 kΩ, 3.35 10^7 kΩ and 1.42 10^{-8} F of R_s, R_P and C, respectively. Fig. 9b represents the real and imaginary parts of the complex impedance as a function of frequency. The peak frequency $\omega_p = 2\pi f_p$ is indicated in both Fig. 9.

Conclusion

Based upon the first principal density function theory (DFT), we have investigated $Al_{0.3}Ga_{0.7}As$ and GaAs for its structure. This study focuses on the analysis of the electronic and optical properties, we have found that these materials are promising candidates for light-absorbing materials in photovoltaic applications due to their optimum direct band gaps, also focus on the effect of p(FSF) and n(BSF)-type window layers of $Al_{0.3}Ga_{0.7}As$ deposited on GaAs substrate, as supported by the evaluation of the optical and electrical properties in the efficiency and the form factor. The $Al_{0.3}Ga_{0.7}As$ exhibits very high absorption. Their form factor increases from 88.35% to 90.35%, the yield from 26.10% to 30.67% and the V_{OC} evolves from 1.02 v to 1.29 v, while the J_{SC} decreases from 28.95 mA/cm^2 to 26.29 mA/cm^2. The $Al_{0.3}Ga_{0.7}As$ presents a wide absorption range in the ultraviolet region. Thus, the

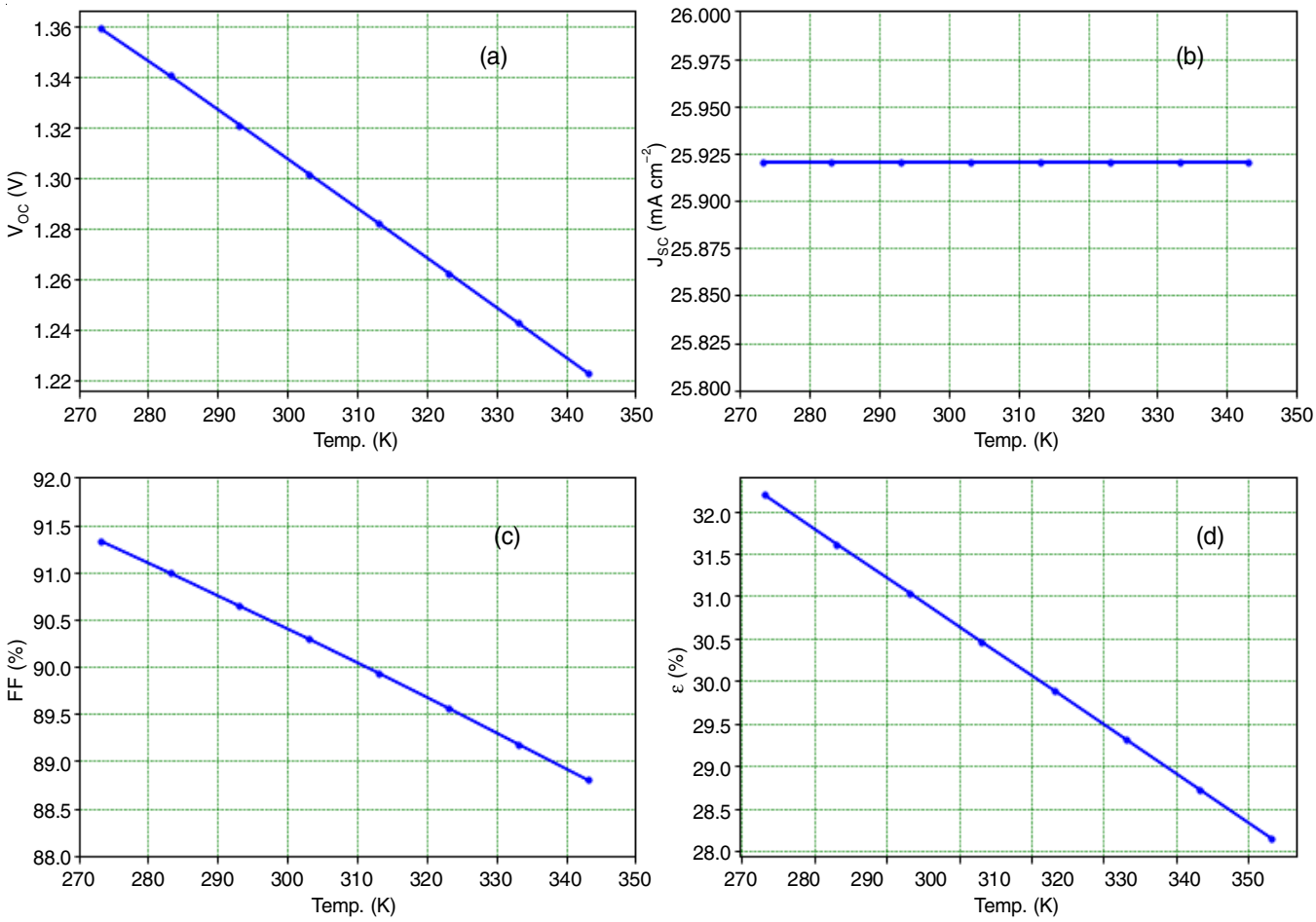

Fig. 8. Effect of temperature on solar cell parameters

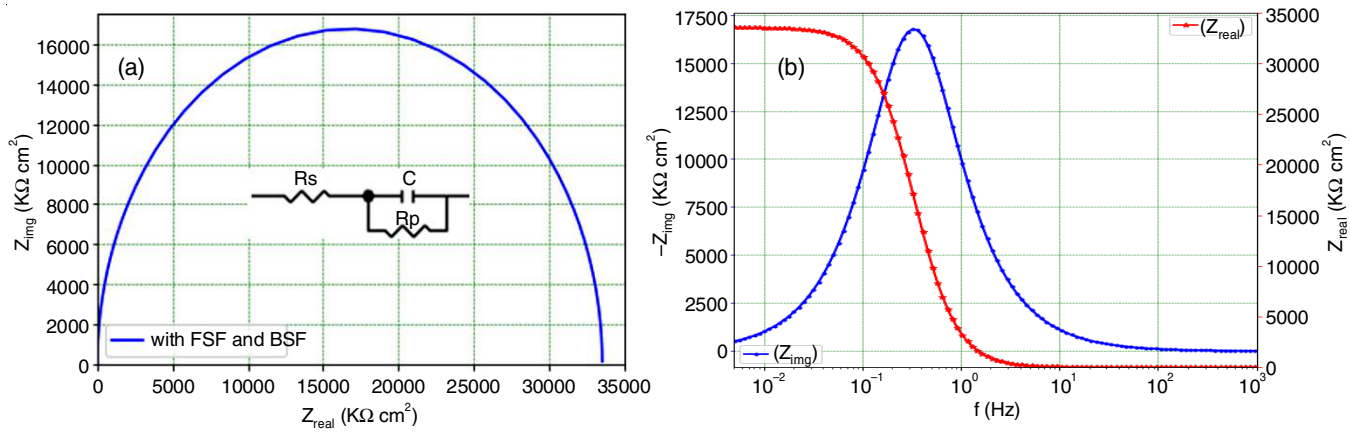

Fig. 9. (a) Nyquist plot of the complex impedance for each frequency and modeled by the Debye equivalent circuit, (b) Real and imaginary parts of the complex impedance as a function of frequency

$Al_{0.3}Ga_{0.7}As$ evokes a good reflection which reaches a value of 39.3%. A new concept of a capacitance and a resistance has been introduced those accounts for the low frequency semi-circle using the impedance spectroscopy method.

CONFLICT OF INTEREST

The authors declare that there is no conflict of interests regarding the publication of this article.

REFERENCES

1. A. Vijayan and J. Prakash, *Green Anal. Chem.*, **3**, 100043 (2022); https://doi.org/10.1016/j.greeac.2022.100043
2. H.S. Salem, M.Y. Pudza and Y. Yihdego, *Sustain. Earth Rev.*, **6**, 10 (2023); https://doi.org/10.1186/s42055-023-00057-4
3. A. El Rharib, A. Amine, A. Oukerroum, M.A. Kinani, Y. Mir and M. Zazoui, *Comput. Condensed Matter.*, **33**, e00744 (2022); https://doi.org/10.1016/j.cocom.2022.e00744
4. D.P. Pham, S. Lee and J. Yi, *Phys. Condensed Matter.*, **611**, 412856 (2021); https://doi.org/10.1016/j.physb.2021.412856

5. M.A. Kinani, R. Chami, A. Lekdadri, A. Elrharib, Y. Mir, E.K. Hlil, A. Amine and M. Zazoui, *Comput. Conden. Matter.*, **26**, e00520 (2021); https://doi.org/10.1016/j.cocom.2020.e00520
6. S. Hwang, S. Kim, H. Cheun, H. Lee, B. Lee, T. Hwang, S. Lee, W. Yoon, H. Lee and B. Park, *Sol. Energy Mater. Sol. Cells*, **155**, 264 (2016); https://doi.org/10.1016/j.solmat.2016.06.009
7. A. Abd-El Mongy, A.A.E. Belal, K. Ali, A.R. Long, *Phys. Status Solidi (a)*, **187**, 575 (2021); https://doi.org/10.1002/1521-396X(200110)187:2<575::AID-PSSA575>3.0.CO;2-2
8. V.P. Kunets, W. Hoerstel, H. Kostial, H. Kissel, U. Müller, G.G. Tarasov, Y.I. Mazur, Z.Y. Zhuchenko and W.T. Masselink, *Sens. Actuators A Phys.*, **101**, 62 (2002); https://doi.org/10.1016/S0924-4247(02)00197-8
9. M. Palummo, M. Re Fiorentin, K. Yamashita, I.E. Castelli and G. Giorgi, *J. Phys. Chem. Lett.*, **14**, 1548 (2023); https://doi.org/10.1021/acs.jpclett.3c00211
10. 10 A. El Rharib, A. Amine, A. Oukerroum, M.A. Kinani, Y. Mir and M. Zazoui, *Computational Conden. Matter*, **33**, e00744 (2022); https://doi.org/10.1016/j.cocom.2022.e00744.
11. A. Mortadi, E. El Hafidi, M. Monkade and R. El Moznine, *Mater. Sci. Energy Technol.*, **7**, 158 (2024); https://doi.org/10.1016/j.mset.2023.10.001
12. E. Chahid, M. Nachaoui, Y. Mir, A. Amine, M.A. Kinani, A. Elrharib, R. Abdia, A. Koumina, A. Malaoui and M. Zazoui, *J. Ovonic Res.*, **18**, 769 (2022); https://doi.org/10.15251/JOR.2022.186.769
13. E.F. Fernández, A. García-Loureiro, N. Seoane and F. Almonacid, *Sol. Energy Mater. Sol. Cells*, **235**, (2022); https://doi.org/10.1016/j.solmat.2021.111483
14. N. Khelfaoui, A. Djafour, C. Ghenai, I. Laib, M.B. Danoune and A. Gougui, *Int. J. Hydrogen Energy*, **46**, 30524 (2021); https://doi.org/10.1016/j.ijhydene.2020.11.193
15. M. Azza, E-H. Chahid, A. Hmairrou, R. Abdia, M. Tridane, A. Malaoui and S. Belaaouad, *Biointerface Res. Appl. Chem.*, **13**, 253 (2023); https://doi.org/10.33263/BRIAC133.253
16. H. Tang, Z. Zhou, S. Jiao, Y. Zhang, S. Li, D. Zhang, J. Zhang, J. Liu and D. Zhao, *Sol. Energy Mater. Sol. Cells*, **235**, 111498 (2022); https://doi.org/10.1016/j.solmat.2021.111498
17. M. Azza, J. Daaif, E.H. Chahid, M. Salah and S. Belaaouad, *E3S Web Conf.*, **297**, 01024 (2021); https://doi.org/10.1051/e3sconf/202129701024
18. P. Ahmed, M.F. Rahman, A.M. Haque, M.K. Mohammed, G.I. Toki and M.H. Ali, **15**, 2 (2023); https://doi.org/doi.org/10.3390/su15021362
19. S. Chakrabarti, A.D. Stiff-Roberts, X.H. Su, P. Bhattacharya, G. Ariyawansa and A.G.U. Perera, *J. Phys. D Appl. Phys.*, **38**, 2135 (2005); https://doi.org/10.1088/0022-3727/38/13/009
20. F. Fares, N. Bouarissa, N.E.H. Fares and F. Mezrag, *Acta Phys. Pol.*, **137**, 4 (2020).
21. P. Schygulla, R. Lang and D. Lackner, *J. Cryst. Growth*, **605**, 127054 (2023); https://doi.org/10.1016/j.jcrysgro.2022.127054
22. M.A. Himi, A. Sghiouri, B. Youbi, Y. Lghazi, A. Amarray, M. Aqil, A. Ouedrhiri, J. Bahar, C. El Haimer, A. Aynaou, L. Hdidou, I. Bimaghra, M. Dahbi and S. El Ghachtouli, *J. Energy Storage*, **61**, 106711 (2023); https://doi.org/10.1016/j.est.2023.106711
23. F. Fabregat-Santiago, G. Garcia-Belmonte, I. Mora-Seró and J. Bisquert., *Phys. Chem. Chem. Phys.*, **13**, 9083 (2011); https://doi.org/10.1039/c0cp02249g